Title

Synthesis of π-Conjugated Chiral Aza/Boracyclophanes with a meta and para Substitution

Journal

Chemistry - A European Journal, 30(5)

ISSN

0947-6539

Authors

Zhang, Kai

Hao, Mengyao

Jin, Tianyun

et al.

Publication Date

2024-01-22

DOI

10.1002/chem.202302950

Peer reviewed

Chemistry–A European Journal
Research Article
doi.org/10.1002/chem.202302950
Chemistry Europe
European Chemical Societies Publishing
www.chemeurj.org

Hot Paper

Synthesis of π-Conjugated Chiral Aza/Boracyclophanes with a *meta* and *para* Substitution

Kai Zhang[+],[a] Mengyao Hao[+],[a, c] Tianyun Jin,[d] Yafei Shi,[a] Guoqing Tian,[a] Chenglong Li,[a] Hongwei Ma,[b] Niu Zhang,[b] Quansong Li,*[a] and Pangkuan Chen*[a]

We herein describe the synthesis of a new class of axially chiral aza/boracyclophanes (**BDN1, BXN1, BDB1 and BXB1**) using binaphthyls as chiral building blocks and the main-group (B/N) chemistry with tunable electronic effects. All macrocycles substituted with triarylamine donors or triarylborane acceptors are strongly luminescent. These macrocycles showed two distinct meta and para π-conjugation pathways, leading to the formation of *quasi* figure-of-eight and square-shaped conformations. Interestingly, comparison of such structural models revealed that the former type of macrocycles **BXN1** and **BXB1** gave higher racemization barriers relative to the other ones. The results reported here may provide a new approach to engineer the optical stability of π-conjugated chiral macrocycles by controlling π-substitution patterns. The ring constraints induced by macrocyclization were also demonstrated to contribute to the configurational persistence as compared with the open-chain analogues ***p*-BTT** and ***m*-BTT**.

Introduction

π-conjugated chiral macrocycles represent one of the research frontiers in the chemistry of carbon nanorings and are of long-standing synthetic interests. Allure of such compounds is attributed not only to the unique electronic structures of twisted π-systems and unusual optoelectronic properties together with their potentials in supramolecular chemistry and material science,[1–5] but also to the fact that cyclization reactions are thermodynamically unfavorable with low isolated yields.[6] Despite substantial challenges arising from the synthesis, quite a few intriguing π-conjugated chiral macrocycles and fully fused nanobelts have been established by previous efforts,[7–16] including application of the concept of inherent planar chirality (with a uniform orientation of the aromatic moieties)[17–24] as well as incorporation of chiral subgroups into the ring skeletons.[25–38] The key advances of π-conjugated chiral macrocycles could also be associated with rapid progresses in chemistry of cycloparaphenylenes (CPPs) since the seminal synthesis in 2008 by *Jasti et al.*[39–46] Not surprisingly thereafter, the design principles rooted in the CPP macrocyclic chemistry have been developed as one of the leading strategies to access carbon-based chiral macrocycles.[47–51]

To further develop macrocyclic chiroptical materials, we envisage the need to reconsider optical persistence that may post an important issue and would thus be a requisite property. In principle, racemization barriers of chiral macrocycles can be considerably enhanced to stabilize their configurations using two approaches: **i**) sterically encumbered substitution effects (e.g. planar chiral pillar[5]arenes[52–55] and pagoda[4]arene[56]) and **ii**) configurational locking via chemical bonding (e.g. metalation in expanded porphyrinoids[57]). Recently, Itami *et al* reported a series of phenanthrene-based chiral macrocycles where systematic tuning of the π-spacers showed a strong influence on the configurational stability of ring structures.[25] Other than these established approaches, our understanding of the effects of π-conjugation pathways still remains limited.

However, the preparation of π-conjugated chiral main-group macrocycles has rarely been achieved heretofore. Compared with all-carbon-based organic materials, the main group heteroatom doped aromatics show particular modulations of the electronic structures and photophysical characteristics.[58–64] To this end, the utilization of electron-deficient organoborane acceptors and/or electron-rich arylamine donors gave rise to highly luminescent π-conjugated systems. In recent years, we and the Jäkle group reported several aza/boracyclophanes with unique dipole-dependent macrocyclic structures and highly tunable optoelectronic properties.[65–71] As shown in Scheme 1, our group has previously reported a highly luminescent organoborane-functionalized

[a] K. Zhang,[+] M. Hao,[+] Y. Shi, G. Tian, C. Li, Prof. Dr. Q. Li, Prof. Dr. P. Chen
Key Laboratory of Photoelectronic/Electrophotonic Conversion Materials
Key Laboratory of Cluster Science of the Ministry of Education, School of Chemistry and Chemical Engineering
Beijing Institute of Technology of China
Beijing, 102488 (China)
E-mail: liquansong@bit.edu.cn
pangkuan@bit.edu.cn
[b] Dr. H. Ma, Dr. N. Zhang
Analysis & Testing Centre
Beijing Institute of Technology
Beijing, 102488 (China)
[c] M. Hao[+]
Program in General Education
Capital Normal University
Beijing, 102488 (China)
[d] T. Jin
Center of Marine Biotechnology and Biomedicine, Scripps Institution of Oceanography
University of California, San Diego
La Jolla, 92093, USA
[+] These authors contributed equally to this work.
Supporting information for this article is available on the WWW under https://doi.org/10.1002/chem.202302950

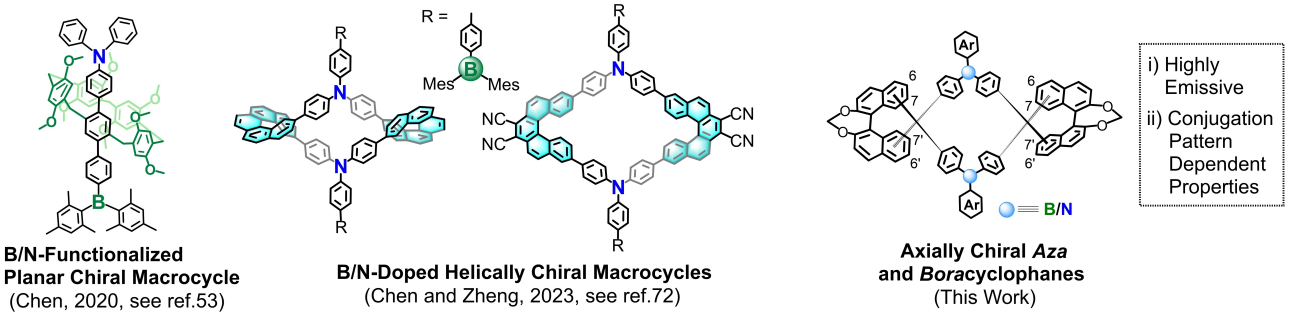

Scheme 1. Representative structures of B/N-doped main-group chiral macrocycles investigated in our group.

planar chiral pillar[5]arene with an emission quantum efficiency up to $\Phi = 99\%$ in THF.[53] More recently, we prepared the first series of chiral organoborane macrocycles with tunable emissions from blue to the near-infrared region, and these [5]helicene-based macrocycles display the unique conjugation-dependent chiral properties.[72] Herein, we propose a new series of π-conjugated axially chiral B/N macrocycles (**BDN1, BDB1, BXN1 and BXB1**) by endocyclic substitution of phenyl groups with binaphthyl moieties as versatile chiral building blocks. These structural models can result in chiral macrocycles with a structural diversity depending on the *meta/para* substitution patterns (the 6,6′- *vs* 7,7′-sites relative to the 9,9′ positions of binaphthyls) and in a distinct pathway to control the optical stability as changes in macrocyclic conformations (i.e., *quasi* figure-of-eight *vs* square shape). Insights into the ring constraints on similar aspects were also obtained when compared with the open-chain analogues ***p*-BTT** and ***m*-BTT**.

Results and Discussion

Synthesis and Characterization

Scheme 2 shows the key steps of the synthetic routes of **BDN1**, **BDB1**, **BXN1** and **BXB1**, and the details are described in Supporting Information (SI). The precursors **1** and **3** (starting

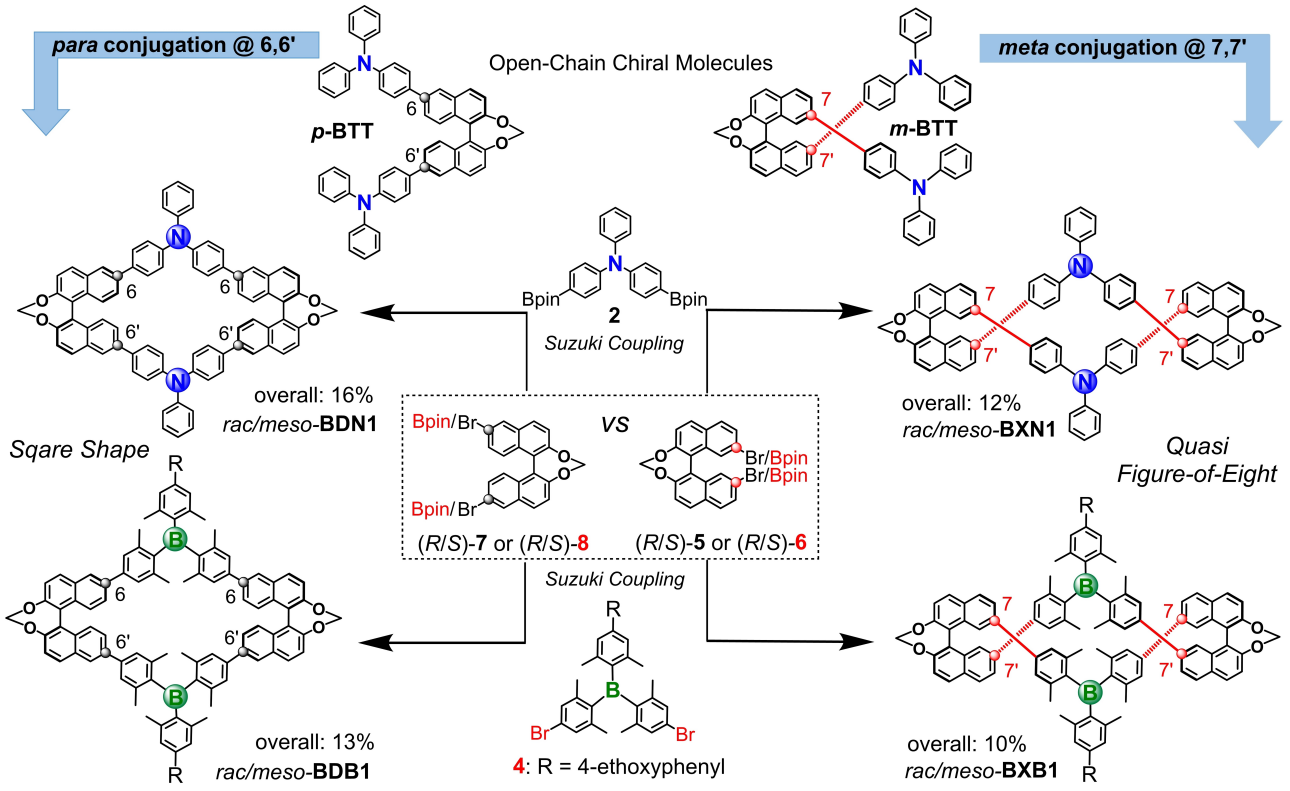

Scheme 2. Key steps of the synthetic approach to macrocycles **BDN1**, **BDB1**, **BXN1 and BXB1**. Reagents and conditions for the Suzuki coupling reactions: $Pd(PPh_3)_4$ (5 mol%), K_2CO_3 (1 M), toluene/EtOH (5/1, v/v) for 24 h under N_2. Bpin = pinacolato. See ref. [73] for the details of open-chain molecules ***p*-BTT** and ***m*-BTT**.

materials for conversion to triarylamine **2** and triarylborane **4**, respectively) as well as the binaphthyl moieties **5** and **7** were prepared according to the previously reported procedures.[74,75] The brominated racemic binaphthyls (*R/S*)-**5** and (*R/S*)-**7** were further converted into (*R/S*)-**6** and (*R/S*)-**8** using diboronic acid pinacol esters in the presence of palladium catalysts. The [2 + 2] Suzuki coupling reactions of **2** with (*R/S*)-**5** or (*R/S*)-**7** gave rise to the triarylamine-substituted macrocycles *rac/meso* **BXN1** and **BDN1** in overall yields of 12% and 16%, respectively. Similarly, the organoborane macrocycles *rac/meso* **BXB1** (10%) and **BDB1** (13%) were also obtained by reacting (*R/S*)-**6** or (*R/S*)-**8** with **4**, respectively.

After the analytically pure products were obtained by using column chromatography, the *meso* (*R,S*)-conformers for **BXN1, BXB1** and **BDN1** were isolated via the reversed phase HPLC. Their resulting (*R,R*)/(*S,S*) racemates as well as the *rac/meso*-**BDB1** were further optically resolved into enantiomers through the preparative chiral HPLC (see SI). Subsequently, the respective enantiopure (*R,R*)- isomers were used for full characterizations by ^{1}H, ^{13}C, ^{11}B NMR and high-resolution mass spectroscopy (HRMS). **BXB1** as an example displayed well-resolved peaks in the aromatic region of ^{1}H NMR spectrum ($CDCl_3$, 25 °C) that can be assigned to protons attached to binaphthyl and Ar_3B moieties in accordance with the symmetric ring structure (Figure 1a). The broad ^{11}B NMR resonances centred at $\delta_B =$ 73 ppm indicate the presence of B_{sp2} acceptors in **BXB1** and **BDB1** (Figures S14 and S16). The successful preparation of macrocycle **BDN1** was also confirmed by high-resolution MALDI-TOF-MS, in which only one single peak was observed at *m/z* 1078.3742, corresponding to the molecular ion (calcd 1078.3765) (Figure 1b; other cycles are shown in Figures S13, S17 and S24). All macrocycles show a high stability for a few weeks both in solution and in the solid state under ambient conditions.

Single crystals of *rac*-**BXN1** and (*R,R*)-**BDB1** for X-ray diffraction analysis were obtained by slow evaporation from CH_2Cl_2/MeOH and CH_2Cl_2/n-hexane, respectively. Figure 2a shows the solid-state structure of **BXN1** with a *quasi* figure-of-eight conformation observed. The two N sites are separated by a distance of 9.139 Å, and the related endocyclic bond angles (119.00(3)°) and 118.35(3)°) are measured close to an optimal value of 120°. In contrast, **BDB1** shows a different square-shaped structure with a much larger cavity size as evidenced by

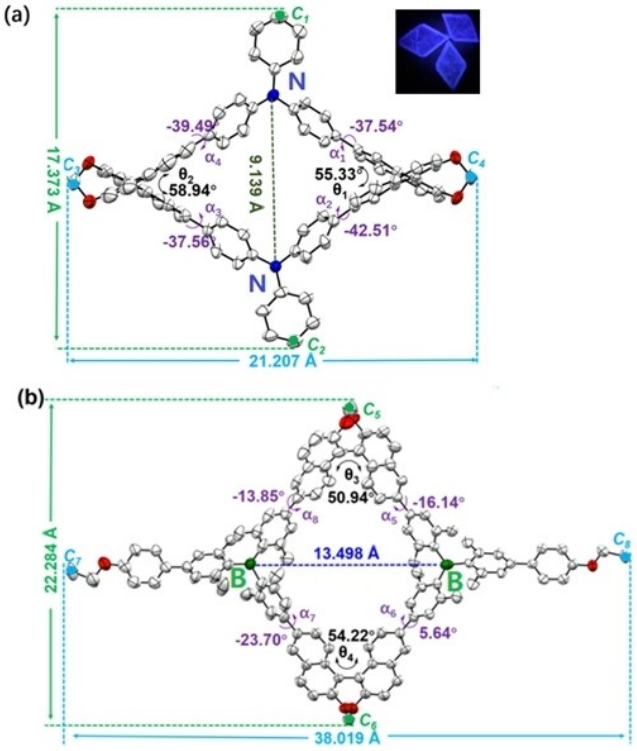

Figure 2. X-ray single crystal structures: (a) ***rac*-BXN1** and (b) **(*R,R*)-BDB1** (C: grey; O:red; 50% thermal probability). Solvent molecules and hydrogen atoms are omitted for clarity. Inset: photograph of the single crystals ***rac*-BXN1** under 365 nm UV-lamp.

a distance of dB…B = 13.498 Å (Figure 2b). Also, the endocyclic bond angles (118.43(3)° and 118.64(3)° against B centers) are slightly smaller than those in **BXN1**. The dihedral angles between the two naphthyl moieties are examined to be $\theta_3 =$ 50.94° and $\theta_4 =$ 54.33° for **BDB1**, and $\theta_1 =$ 55.33° and $\theta_2 =$ 58.94° for **BXN1**. The differences in these angles are suggestive of a less strained structure for the *quasi* figure-of-eight macrocycles with *meta* π-conjugation.

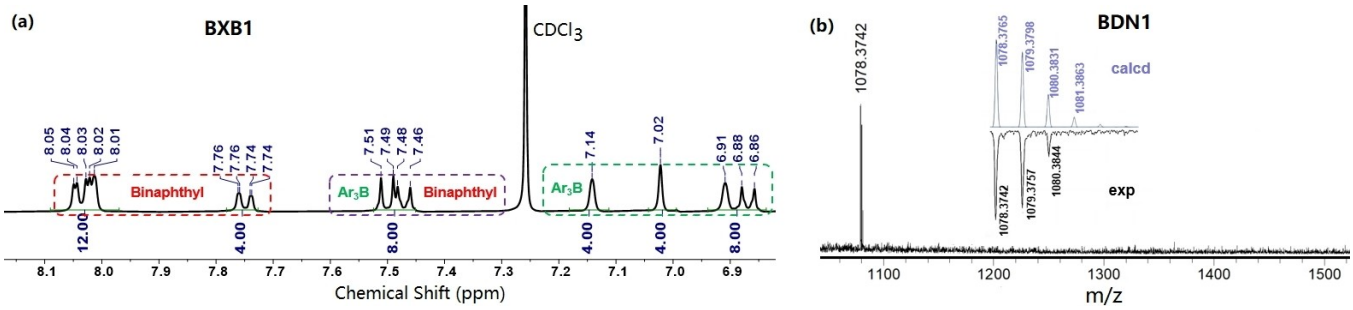

Figure 1. (a) Aromatic region of the ^{1}H NMR spectrum for **BXB1** (400 MHz, $CDCl_3$, 25 °C). (b) MALDI-TOF mass spectrum (positive-ion mode) of **BDN1** showing experimental and simulated isotopic patterns.

Photophysical Properties and Electronic Structures

In the UV/Vis absorption spectra, these chiral macrocycles exhibit similar absorption bands of π–π^* transitions in the range of 334–363 nm without solvent dependence. They show strong emissions in CH_2Cl_2 with a high quantum yield ($\Phi = 0.81$, 0.53, 0.82, 0.81 for **BDN1, BDB1, BXN1 BXB1**, respectively; Figure 3a, and Tables S3–S7), and the solvatochromic shifts in the emissions were observed due to intramolecular charge transfer (ICT, Figure S28). Variable-temperature (VT) emission spectra reflected the thermochromic properties of macrocycles in response to changes in temperature as an external stimulus (Figure S31). As T is increased from 150 to 345 K, the thermally-induced hypsochromic shifts of the emission maximum are attributed to the variable stabilization of the ICT states as a result of the T-dependent polarity of solvents. Luminescence in the solid states ($\Phi_S = 0.20$–0.34) may lead to potential applications in optoelectronic devices.

DFT computations have revealed the degenerate N-centred HOMO/HOMO-1 and binaphthyl-delocalized LUMO/LUMO + 1 in **BDN1**, while the related two moieties are involved in the HOMO or LUMO for **BXN1**. In **BDB1**, the HOMO is dominated by binaphthyls and the LUMO is centred on B acceptors (Figure 3c). **BXB1** shows the HOMO with contributions both from the binaphthyls and the exocyclic phenyl rings on B, while the LUMO is nearly delocalized over the B-bridged ring skeleton. Each of the electronic transitions to S_1, S_2, S_3, S_4, S_5 and S_6 is attributed to vertical excitations to the LUMO, LUMO + 1 and LUMO + 2 from the HOMO, HOMO-1 and HOMO-2, all giving rise to a charge transfer character. The cyclic voltammetry (CV) scans of **BDN1** and **BXN1** showed reversible two-electron oxidation waves with a half-wave potential at $E^{ox}_{1/2} = +0.49$ and +0.45 V (*vs* Fc+/Fc, in CH_2Cl_2), respectively, corresponding to the oxidations of N sites. In contrast, **BDB1** and **BXB1** exhibited a reversible two-electron reduction band at $E^{red}_{1/2} = -2.36$ and −2.32 V in THF, respectively, due to the reduction of electron-deficient boron centers (Figure S32).

Each pair of the enantiomers showed a high enantiomeric excess (> 98% *ee*, Table S8), and their absolute configurations were determined either by X-ray crystallography (Figure 2b) or simulated ECD spectra (CAM-B3LYP/6-31G(d,p), Figure S46). First, kinetic studies of thermal racemization were performed for the open-chain molecules. As shown in Figure 4a, the *ee* value for (*S*)-***p*-BTT** was gradually decreased upon thermal treatment as the conversion to (*R*)-***p*-BTT** conformer in o-dichlorobenzene (o-DCB) (Figure S37a). Temperature-dependent *ee* values were monitored by HPLC at 130–150 °C. The rate constants (k) obtained by equation ($\ln([ee]t/[ee]0) = -2kt$) were plotted versus the reciprocal number of temperature ($1/T$). Fitting of the data in Eyring plot gave racemization barrier $\Delta G^{\ddagger}_{(298K)} = 32.93$ kcal mol^{-1} with the thermodynamic parameters $\Delta H^{\ddagger} = 32.85$ kcal mol^{-1} and $\Delta S^{\ddagger} = -0.26$ cal mol^{-1} K^{-1} (Figure S38). In comparison, similar studies for (*R*)-***m*-BTT** gave rise to a larger barrier $\Delta G^{\ddagger} = 35.32$ kcal mol^{-1} ($\Delta H^{\ddagger} = 33.61$ kcal mol^{-1} and $\Delta S^{\ddagger} = -5.74$ cal mol^{-1} K^{-1}). This is in accordance with a racemization process of the latter at higher T > 160 °C (Figure 4b and S37b).

For the square-shaped chiral macrocycles (*S,S*)-**BDN1** and (*S,S*)-**BDB1**, we observed two sets of new peaks in HPLC traces upon heating at 175 °C and 168 °C, respectively. The existence of enantiomeric and *meso* forms (Figure S39) likely indicates a sequential two-step isomerization of the two binaphthyl units. The time-dependent kinetic studies showed an increased amount of the new fractions as evidenced by the relative intensities ($I/I_{(S,S)\text{-BDN1 or BDB1}}$, Figure S40). In sharp contrast, no racemization was experimentally observed at all in the *quasi* figure-of-eight (*R,R*)-**BXN1** and (*R,R*)-**BXB1** up to 180 °C (Figure S39c and S39d). When compared with the respective open-

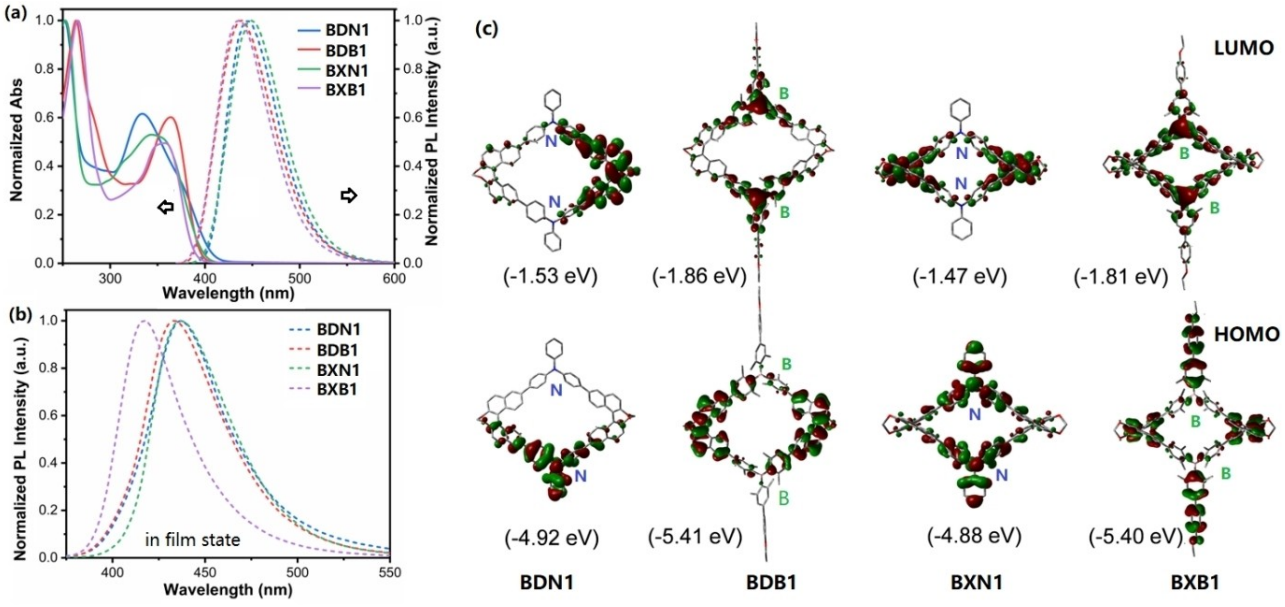

Figure 3. Absorption and emission spectra: (a) in CH_2Cl_2 (1.0×10^{-5} M, under N_2, $\lambda_{ex} = \lambda_{abs,max}$) and (b) in the solid state at 298 K. (c) DFT-optimized structures and frontier molecular orbital plots of **BDN1, BDB1, BXN1** and **BXB1** (iso = 0.02, B3LYP/6-31G).

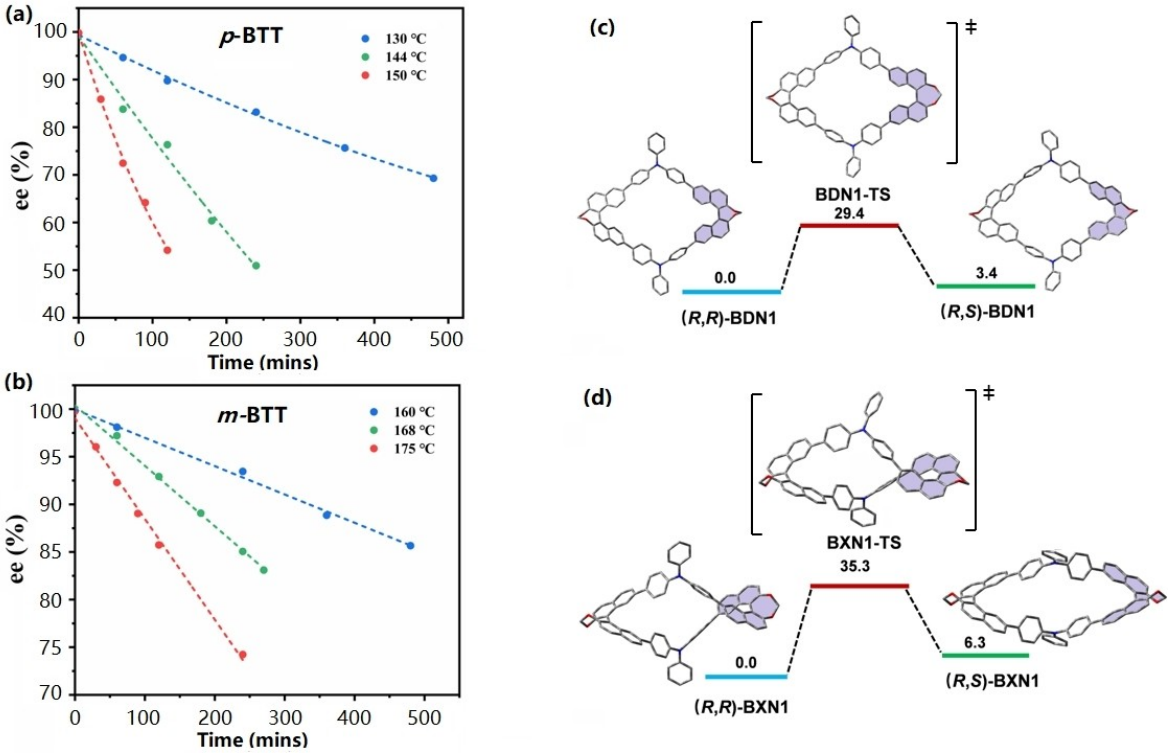

Figure 4. (a, b) Temperature-dependent *ee* ratio of enantioenriched (*S*)-***p*-BTT** and (*R*)-***m*-BTT** in 1,2-dichlorobenzene. (c, d) Isomerization process of the **BDN1** and **BXN1** from (*R,R*)- to (*R,S*)-isomer with the relative Gibbs free energy (kcal mol^{-1}) calculated at the B3LYP/6-31G(d) level.

chain (*R*)-***p*-BTT** and (*R*)-***m*-BTT**, racemizations of (*S,S*)-**BDN1** and (*R,R*)-**BXN1** were found to proceed at higher T. They are suggestive of larger racemization barriers for macrocyclic systems, which could be attributed to the impact of ring constraints on the configurational stability. Time-dependent residual fractions revealed that (*R*)-***m*-BTT** is configurationally more stable than (*S,S*)-**BDN1** (Figure S42). The experimental results from kinetic studies lead to a tunable optical stability in the order **BXN1** > **m-BTT** > **BDN1** > ***p*-BTT** as well as **BXB1** > **BDB1**.

Racemization barriers of all chiral macrocycles were predicted by computational studies (B3LYP/6-31G(d)). Incorporation of two binaphthyl moieties into macrocycles provides three stereomers: the racemic (*R,R*)/(*S,S*) isomers and *meso*-(*R,S*) form. Calculated homochiral (*R,R*)-isomers are all thermodynamically more stable than the *meso*-(*R,S*) forms with a larger difference of Gibbs free energy for **BXN1** (6.3 kcal/mol) and **BXB1** (7.0 kcal/mol) in comparison to **BDN1** (3.4 kcal/mol) and **BDB1** (3.4 kcal/mol). Figure 4 and Figure S51 exhibit the proposed isomerization from (*R,R*)-isomers to the *meso*-(*R,S*) conformers through a transition state (*TS*) with the two extremities of binaphthyls oriented face-to-face and confirmed by the intrinsic reaction coordinate (IRC) calculations. The computational racemization barriers were determined to be 29.4, 29.4, 35.3 and 38.4 kcal/mol for **BDN1, BDB1, BXN1** and **BXB1**, respectively, in line with the trend derived from thermally-controlled kinetic studies, similar to the trend observed in our [5]helicene-based chiral macrocycles.[72]

The chiroptical properties in the ground state were investigated by circular dichroism (CD) spectroscopy in CH_2Cl_2 ($c = 1.0\times10^{-5}$ M). Figure 5 shows clearly the mirror-image CD spectra with strong Cotton effects. The anisotropy factors associated with the most red-shifted Cotton effect ($|g_{abs}|$, defined as $\Delta\varepsilon/\varepsilon$) were estimated to be 2.91×10^{-3} (364 nm), 1.46×10^{-3} (364 nm), 3.79×10^{-3} (341 nm) and 5.00×10^{-3} (363 nm) for **BDN1**, **BDB1**, **BXN1** and **BXB1**, respectively. These values are comparable to or slightly higher than those of the open-chain ***p*-BTT** ($|g_{abs}| = 7.11\times10^{-4}$, 364 nm) and ***m*-BTT** ($|g_{abs}| = 7.60\times10^{-3}$, 373 nm).[73] The dissymmetry factors were also theoretically calculated by the equation $g_{abs} = 4\cos\theta|m||\mu|/(|m|^2+|\mu|^2)$, wherein μ, m, and θ represent the electric and magnetic transition dipole moments, as well as the angle between μ and m, respectively (Figure 5). The $|g_{abs}|$ values were estimated to be 5.67×10^{-3}, 0.898×10^{-3}, 3.01×10^{-3} and 8.07×10^{-3} for the lowest-energy absorption peak ($S_0\rightarrow S_1$, B3LYP/6-31G(d,p)) of **BDN1**, **BDB1**, **BXN1** and **BXB1**, respectively, in good agreement with the experimental results.

Their chiroptical properties in the excited state were characterized by circularly polarized luminescence (CPL) spectra. As shown in Figure S43, all chiral macrocycles displayed mirror images of the CPL profiles in solution ($c = 1.0\times10^{-5}$ M), and a gradual redshift was observed in the spectra with increasing solvent polarity, in line with the solvatochromic shifts in their emissions due to a charge-transfer character. The luminescence dissymmetry factors $|g_{lum}|$ were examined to be in the range of 1.0×10^{-4} to 4.08×10^{-3} (Table S9 and S10). According to a recently proposed concept, the CPL brightness (B_{CPL} =

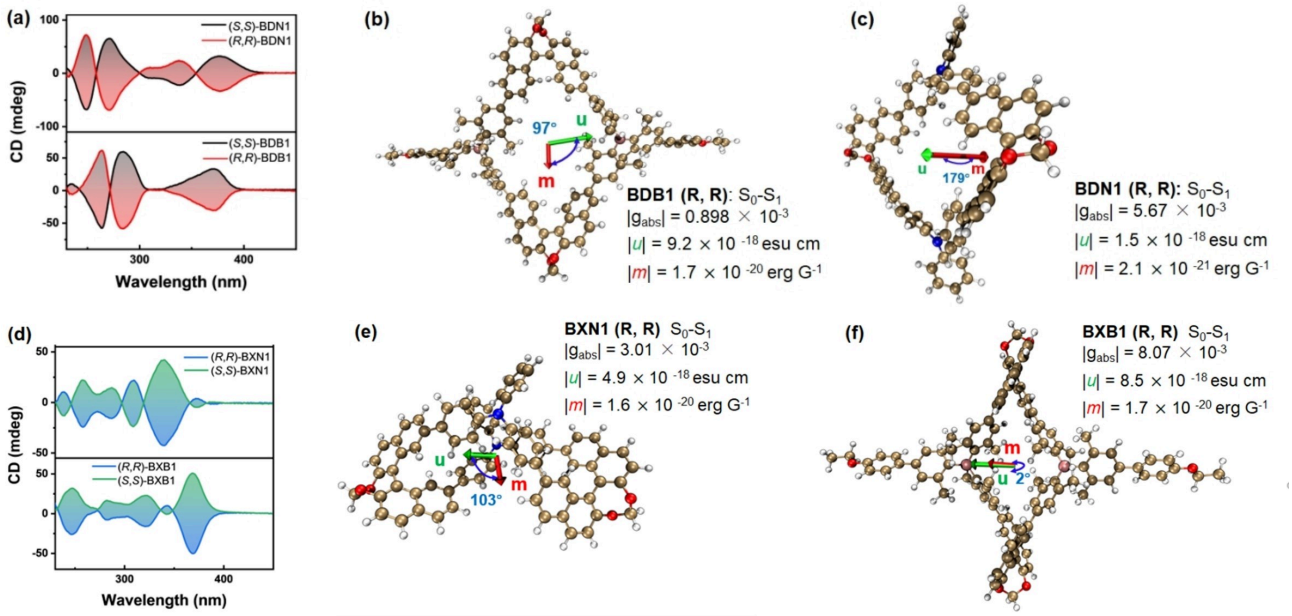

Figure 5. (a, d) CD spectra of enantiomers of chiral macrocycles in CH_2Cl_2 ($c = 1.0\times10^{-5}$ M) under N_2 at 298 K. (b, c, e, f) The electric transition dipole moments (μ, green) and magnetic dipole moments (m, red) calculated for the lowest-energy transitions ($S_0 \rightarrow S_1$, B3LYP/6-31G(d,p)) of all chiral macrocycles.

$\varepsilon\times\Phi_{PL}\times g_{lum}/2$)[76] has been quantified to be 27.7, 6.7, 3.7 and 35.7 $M^{-1}cm^{-1}$ for **BDN1, BDB1, BXN1** and **BXB1**, respectively. They indicate that the *quasi* figure-of-eight organoborane macrocycle **BXB1** would show the best overall performance as CP-light emitting materials. The g_{lum} and B_{CPL} values in these cases are quite comparable to those reported for other chiral cyclophanes and nanobelts (Figure S52 and Table S30).

With the experimental data both of $|g_{abs}|$ and $|g_{lum}|$ in hand, it is possible to correlate the ground- and excited-state chiroptical properties as a function of the conjugation patterns (*meta* vs *para* substitution). All the macrocycles and open-chain analogues show smaller $|g_{lum}|$ values than $|g_{abs}|$, consistent with the general trend for organic chiral molecules due to conformational relaxation in the excited states. A closer inspection of the g_{lum}–g_{abs} plots revealed that the group of *meta* conjugated molecules slightly differ from the *para* conjugated. As shown in Figure 6, regression analysis of the plot for **BDN1, BDB1** and ***p*-BTT** gave a significant correlation with $R^2 = 0.944$ as the result of the structurally rigid π-systems.[77,78] In contrast, the smaller slope of the data fitting for **BXN1, BXB1** and ***m*-BTT** may reflect a higher degree of conformational flexibility as well as a larger difference in the ground/excited state geometry of the *meta* substituted compounds reported herein.

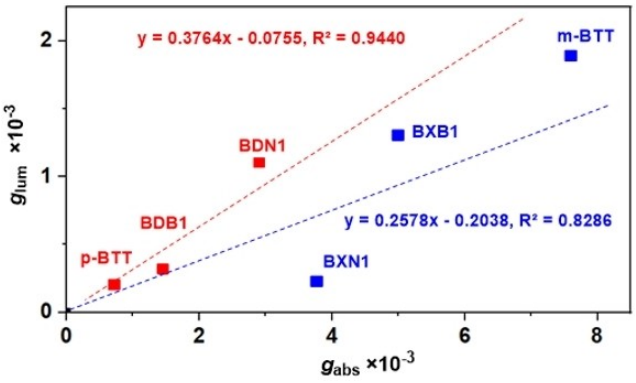

Figure 6. Correlation of the emission and absorption dissymmetry factors by linear fitting of the data for *meta* conjugated (blue: **BXN1, BXB1** and ***m*-BTT**) *vs para* conjugated chiral systems (red: **BDN1, BDB1** and ***p*-BTT**).

Conclusions

We have described the new structural models of π-conjugated chiral main-group B/N macrocycles via aryl substitution with chiral building blocks. This series of chiral aza/boracyclophanes showed two distinct conformations that involve the *quasi* figure-of-eight macrocycles (**BXN1**, **BXB1**) and square-shaped ones (**BDN1**, **BDB1**). The unique structures were derived from the different substitution patterns either at the *para* 6,6′ or *meta* 7,7′ positions of binaphthyl moieties. DFT computations together with kinetic studies reveal that the figure-of-eight topology can provide a higher optical stability than the square-shaped macrocycles, and that the ring constraints (*versus* the open-chain analogues) also contribute significantly. The results are further evidenced by the racemization energy barriers in a trend ***p*-BTT** < **BDN1** < ***m*-BTT** < **BXN1** as well as **BDB1** < **BXB1**. Our discovery may offer a distinct approach to access highly luminescent main-group chiral macrocycles by engineering the ring conformation to address the critical issue of configurational stability.

Supporting Information

Experimental procedures, analytical data (^{1}H, ^{13}C, ^{11}B NMR and HRMS) for products and intermediates, crystallography, optical resolution, photophysical and chiroptical data, and DFT computations.

Deposition Numbers 2181916 (*rac*-BXN1) and 2181917 ((*R, R*)-BDB1) contain the supplementary crystallographic data for this paper. These data are provided free of charge by the joint Cambridge Crystallographic Data Centre and Fachinformationszentrum Karlsruhe Access Structures service.

Acknowledgements

P. C and Q. L acknowledge the financial support of National Natural Science Foundation of China (No. 22271013, 21772012, 22173008) and Beijing Natural Science Foundation (No. 2232024). We are greatly thankful to Prof. Suning Wang at Queen's University for helpful discussions over the years. We thank the Analysis & Testing Centre at Beijing Institute of Technology for advanced facilities.

Conflict of Interests

The authors declare no conflict of interest to report.

Data Availability Statement

The data that support the findings of this study are available from the corresponding author upon reasonable request.

Keywords: π-Conjugated Macrocycles · Axial Chirality · Circularly Polarized Luminescence · Organoborane · Triarylamine

[1] M. Iyoda, J. Yamakawa, M. J. Rahman, *Angew. Chem. Int. Ed.* **2011**, *50*, 10522–10553; *Angew. Chem.* **2011**, *123*, 10708–10740.
[2] Q. H. Guo, Y. Y. Qiu, M. X. Wang, J. F. Stoddart, *Nat. Chem.* **2021**, *13*, 402–419.
[3] C. Liu, Y. Ni, X. Lu, G. Li, J. Wu, *Acc. Chem. Res.* **2019**, *52*, 2309–2321.
[4] M. Iyoda, H. Shimizu, *Chem. Soc. Rev.* **2015**, *44*, 6411–6424.
[5] R. López, C. Palomo, *Angew. Chem. Int. Ed.* **2022**, *61*, e202113504.
[6] F. Schlütter, F. Rossel, M. Kivala, V. Enkelmann, J.-P. Gisselbrecht, P. Ruffieux, R. Fasel, K. Müllen, *J. Am. Chem. Soc.* **2013**, *135*, 4550–4557.
[7] For a recent review, see: M. Hasegawa, Y. Nojima, Y. Mazaki, *ChemPhotoChem* **2021**, *5*, 1042–1058.
[8] K. Campbell, R. R. Tykwinski, M. M. Haley, R. R. Tykwinski, Eds. Carbon-Rich Compounds: From Molecules to Materials,Wiley-VCH Verlag GmbH & Co. KGaA: Weinheim, Germany, **2006**; pp 229–294.
[9] K. Y. Cheung, S. Gui, C. Deng, H. Liang, Z. Xia, Z. Liu, L. Chi, Q. Miao, *Chem* **2019**, *5*, 838–847.
[10] A. Yagi, Y. Segawa, K. Itami, *Chem* **2019**, *5*, 746–748.
[11] J. Nogami, Y. Tanaka, H. Sugiyama, H. Uekusa, A. Muranaka, M. Uchiyama, K. Tanaka, *J. Am. Chem. Soc.* **2020**, *142*, 9834–9842.
[12] W. Fan, T. Matsuno, Y. Han, X. Wang, Q. Zhou, H. Isobe, J. Wu, *J. Am. Chem. Soc.* **2021**, *143*, 15924–15929.
[13] M. Krzeszewski, H. Ito, K. Itami, *J. Am. Chem. Soc.* **2022**, *144*, 862–871.
[14] Y. Segawa, T. Watanabe, K. Yamanoue, M. Kuwayama, K. Watanabe, J. Pirillo, Y. Hijikata, K. Itami, *Nat. Synth.* **2022**, *1*, 535–541.
[15] W. Fan, T. M. Fukunaga, S. F. Wu, Y. Han, Q. F. Zhou, J. Y. Wang, Z. T. Li, X. D. Hou, H. P. Wei, Y. Ni, H. Isobe, J. S. Wu, *Nat. Synth.* **2023**. Doi: 10.1038/s44160-023-00317-3.
[16] J. H. Chen, Z. Y. Jiang, H. Xiao, S. Tong, T. H. Shi, J. P. Zhu, M. X. Wang, *Angew. Chem. Int. Ed.* **2023**, *62*, e202301782.
[17] S. Hitosugi, W. Nakanishi, T. Yamasaki, H. Isobe, *Nat. Commun.* **2011**, *2*, 492.
[18] J. Wang, G. Zhuang, M. Chen, D. Lu, Z. Li, Q. Huang, H. Jia, S. Cui, X. Shao, S. Yang, P. Du, *Angew. Chem. Int. Ed.* **2020**, *59*, 1619–1626.
[19] G. E. Arnott, *Chem. Eur. J.* **2018**, *24*, 1744–1754.
[20] T. Miura, T. Nakamuro, Y. Ishihara, Y. Nagata, M. Murakami, *Angew. Chem. Int. Ed.* **2020**, *59*, 20475–20479.
[21] S. Tong, J. T. Li, D. D. Liang, Y. E. Zhang, Q. Y. Feng, X. Zheng, J. P. Zhu, M. X. Wang, *J. Am. Chem. Soc.* **2020**, *142*, 14432–14436.
[22] L. Zhang, G. L. Zhang, H. Qu, Y. Todarwal, Y. Wang, P. Norman, M. Linares, M. Surin, H. J. Zhang, J. B. Lin, Y. B. Jiang, *Angew. Chem. Int. Ed.* **2021**, *60*, 24543–24548.
[23] W. Xu, Y. Nagata, N. Kumagai, *J. Am. Chem. Soc.* **2023**, *145*, 2609–2618.
[24] Y. Q. Fan, J. He, L. Liu, G. Q. Liu, S. Z. Guo, Z. Lian, X. N. Li, W. J. Guo, X. B. Chen, Y. Wang, H. Jiang, *Angew. Chem. Int. Ed.* **2023**, *62*, e202304623.
[25] Y. Li, A. Yagi, K. Itami, *J. Am. Chem. Soc.* **2020**, *142*, 3246–3253.
[26] G. Li, T. Matsuno, Y. Han, H. Phan, S. Wu, Q. Jiang, Y. Zou, H. Isobe, J. Wu, *Angew. Chem. Int. Ed.* **2020**, *59*, 9727–9735.
[27] F. Sannicolò, P. R. Mussini, T. Benincori, R. Cirilli, S. Abbate, S. Arnaboldi, S. Casolo, E. Castiglioni, G. Longhi, R. Martinazzo, M. Panigati, M. Pappini, E. Procopio, S. Rizzo, *Chem. Eur. J.* **2014**, *20*, 15298–15302.
[28] K. Sato, M. Hasegawa, Y. Nojima, N. Hara, T. Nishiuchi, Y. Imai, Y. Mazaki, *Chem. Eur. J.* **2021**, *27*, 1323–1329.
[29] M. Hasegawa, C. Hasegawa, Y. Nagaya, K. Tsubaki, Y. Mazaki, *Chem. Eur. J.* **2022**, *28*, e202202218.
[30] L. Zhang, G. Zhang, H. Qu, Y. Todarwal, Y. Wang, P. Norman, M. Linares, M. Surin, H. J. Zhang, J. Lin, Y.-B. Jiang, *Angew. Chem. Int. Ed.* **2021**, *60*, 24543–24548.
[31] J. Malinčík, S. Gaikwad, J. P. Mora-Fuentes, M. A. Boillat, A. Prescimone, D. Häussinger, A. G. Campaña, T. Šolomek, *Angew. Chem. Int. Ed.* **2022**, *61*, e202208591.
[32] W. Xu, X. D. Yang, X. B. Fan, X. Wang, C. H. Tung, L. Z. Wu, H. Cong, *Angew. Chem. Int. Ed.* **2019**, *58*, 3943–3947.
[33] Y. Nojima, M. Hasegawa, N. Hara, Y. Imai, Y. Mazaki, *Chem. Eur. J.* **2021**, *27*, 5923–5929.
[34] P. Fang, M. Chen, X. Zhang, P. Du, *Chem. Commun.* **2022**, *58*, 8278–8281.
[35] M. Ball, B. Fowler, P. Li, L. A. Joyce, F. Li, T. F. Liu, D. Paley, Y. Zhong, H. X. Li, S. X. Xiao, F. Ng, *J. Am. Chem. Soc.* **2015**, *137*, 9982–9987.
[36] X. Jiang, J. D. Laffoon, D. Chen, S. Pérez-Estrada, A. S. Danis, J. Rodríguez-López, M. A. Garcia-Garibay, J. Zhu, J. S. Moore, *J. Am. Chem. Soc.* **2020**, *142*, 6493–6498.
[37] G. R. Kiel, K. L. Bay, A. E. Samkian, N. J. Schuster, J. B. Lin, R. C. Handford, C. Nuckolls, K. N. Houk, T. D. Tilley, *J. Am. Chem. Soc.* **2020**, *142*, 11084–11091, and references therein.
[38] J. Malinčík, S. Gaikwad, J. P. Mora-Fuentes, M. A. Boillat, A. Prescimone, D. Häussinger, A. G. Campaña, T. Šolomek, *Angew. Chem. Int. Ed.* **2022**, *61*, e2022085.
[39] R. Jasti, J. Bhattacharjee, J. B. Neaton, C. R. Bertozzi, *J. Am. Chem. Soc.* **2008**, *130*, 17646–17647.
[40] H. Omachi, S. Matsuura, Y. Segawa, K. Itami, *Angew. Chem. Int. Ed.* **2010**, *49*, 10202–10205.
[41] T. J. Sisto, M. R. Golder, E. S. Hirst, R. Jasti, *J. Am. Chem. Soc.* **2011**, *133*, 15800–15802.
[42] T. Iwamoto, Y. Watanabe, Y. Sakamoto, T. Suzuki, S. Yamago, *J. Am. Chem. Soc.* **2011**, *133*, 8354–8361.
[43] F. E. Golling, M. Quernheim, M. Wagner, T. Nishiuchi, K. Müllen, *Angew. Chem. Int. Ed.* **2014**, *53*, 1525–1528.
[44] Z. A. Huang, C. Chen, X. D. Yang, X. B. Fan, W. Zhou, C. H. Tung, L. Z. Wu, H. Cong, *J. Am. Chem. Soc.* **2016**, *138*, 11144–11147.
[45] Q. Huang, G. L. Zhuang, M. M. Zhang, J. Y. Wang, S. D. Wang, Y. Y. Wu, S. F. Yang, P. W. Du, *J. Am. Chem. Soc.* **2019**, *141*, 18938–18943.
[46] M. Hermann, D. Wassy, B. Esser, *Angew. Chem. Int. Ed.* **2021**, *60*, 15743–15766.
[47] K. Senthilkumar, M. Kondratowicz, T. Lis, P. J. Chmielewski, J. Cybińska, J. L. Zafra, J. Casado, T. Vives, J. Crassous, L. Favereau, M. Stępień, *J. Am. Chem. Soc.* **2019**, *141*, 7421–7427.
[48] T. A. Schaub, E. A. Prantl, J. Kohn, M. Bursch, C. R. Marshall, E. J. Leonhardt, T. C. Lovell, L. N. Zakharov, C. K. Brozek, S. R. Waldvogel, S. Grimme, R. Jasti, *J. Am. Chem. Soc.* **2020**, *142*, 8763–8775.

[49] L. H. Wang, N. Hayase, H. Sugiyama, J. Nogami, H. Uekusa, K. Tanaka, *Angew. Chem. Int. Ed.* **2020**, *59*, 17951–17957.
[50] X. Zhang, H. Liu, G. Zhuang, S. Yang, P. Du, *Nat. Commun.* **2022**, *13*, 3543.
[51] Q. F. Zhou, X. D. Hou, J. Y. Wang, Y. Ni, W. Fan, Z. T. Li, X. Wei, K. Li, W. Yuan, Z. F. Xu, M. Z. Zhu, Y. L. Zhao, Z. Sun, J. S. Wu, *Angew. Chem. Int. Ed.* **2023**, *62*, e202302266.
[52] T. Ogoshi, K. Masaki, R. Shiga, K. Kitajima, T. Yamagishi, *Org. Lett.* **2011**, *13*, 1264–1266.
[53] J. Chen, X. Yin, B. Wang, K. Zhang, G. Meng, S. Zhang, Y. Shi, N. Wang, S. Wang, P. Chen, *Angew. Chem. Int. Ed.* **2020**, *59*, 11267–11272.
[54] H. Zhu, Q. Li, B. Shi, H. Xing, Y. Sun, S. Lu, L. Shangguan, X. Li, F. Huang, P. J. Stang, *J. Am. Chem. Soc.* **2020**, *142*, 17340–17345.
[55] W. J. Li, Q. Gu, X. Q. Wang, D. Y. Zhang, Y. T. Wang, X. He, W. Wang, H.-B. Yang, *Angew. Chem. Int. Ed.* **2021**, *60*, 9507–9515.
[56] X. N. Han, Y. Han, C. F. Chen, *J. Am. Chem. Soc.* **2020**, *142*, 8262–8269.
[57] K. Liang, H. Chen, X. Wang, T. Lu, Z. Duan, J. L. Sessler, C. H. Lei, *Angew. Chem. Int. Ed.* **2022**, *61*, e202212770, and references therein.
[58] M. Stępień, E. Gońka, M. Żyła, N. Sprutta, *Chem. Rev.* **2017**, *117*, 3479–3716.
[59] M. Hirai, N. Tanaka, M. Sakai, S. Yamaguchi, *Chem. Rev.* **2019**, *119*, 8291–8331.
[60] K. Dhbaibi, L. Favereau, J. Crassous, *Chem. Rev.* **2019**, *119*, 8846–8953.
[61] X. Su, T. A. Bartholome, J. R. Tidwell, A. Pujol, S. Yruegas, J. J. Martinez, C. D. Martin, *Chem. Rev.* **2021**, *121*, 4147–4192.
[62] F. Vidal, F. Jäkle, *Angew. Chem. Int. Ed.* **2019**, *58*, 5846–5870.
[63] S. K. Bose, L. Mao, L. Kuehn, U. Radius, J. Nekvinda, W. L. Santos, S. A. Westcott, P. G. Steel, T. B. Marder, *Chem. Rev.* **2021**, *121*, 13238–13341.
[64] L. Ji, S. Griesbeck, T. B. Marder, *Chem. Sci.* **2017**, *8*, 846–863.
[65] P. Chen, F. Jäkle, *J. Am. Chem. Soc.* **2011**, *133*, 20142–20145.
[66] P. Chen, R. A. Lalancette, F. Jäkle, *Angew. Chem. Int. Ed.* **2012**, *51*, 7994–7998.
[67] P. Chen, X. Yin, N. Baser-Kirazli, F. Jäkle, *Angew. Chem. Int. Ed.* **2015**, *54*, 10768–10772.
[68] N. Baser-Kirazli, R. A. Lalancette, F. Jäkle, *Angew. Chem. Int. Ed.* **2020**, *59*, 8689–8697.
[69] D. Shimoyama, N. Baser-Kirazli, R. A. Lalancette, F. Jäkle, *Angew. Chem. Int. Ed.* **2021**, *60*, 17942–17946.
[70] Y. W. Jia, P. F. Li, K. L. Liu, C. L. Li, M. Y. Liu, J. Q. Di, N. Wang, X. Yin, N. Zhang, P. Chen, *Chem. Sci.* **2022**, *13*, 11672–11679.
[71] P. Li, D. Shimoyama, N. Zhang, Y. Jia, G. Hu, C. Li, X. Yin, N. Wang, F. Jäkle, P. Chen, *Angew. Chem. Int. Ed.* **2022**, *61*, e202200612.
[72] F. Zhao, J. Zhao, H. Liu, Y. Wang, J. X. Duan, C. L. Li, J. Q. Di, N. Zhang, X. Y. Zheng, P. Chen, *J. Am. Chem. Soc.* **2023**, *145*, 10092–10103.
[73] K. Zhang, J. Zhao, N. Zhang, J. F. Chen, N. Wang, X. Yin, X. Zheng, P. Chen, *J. Mater. Chem. C* **2022**, *10*, 1816–1824.
[74] J. W. Park, M. D. Ediger, M. M. Green, *J. Am. Chem. Soc.* **2001**, *123*, 49–56.
[75] K. Takaishi, S. Hinoide, T. Matsumoto, T. Ema, *J. Am. Chem. Soc.* **2019**, *141*, 11852–11857.
[76] L. Arrico, L. Di Bari, F. Zinna, *Chem. Eur. J.* **2021**, *27*, 2920–2934.
[77] H. Tanaka, Y. Inoue, T. Mori, *ChemPhotoChem.* **2018**, *2*, 386–402.
[78] M. Cei, L. Di Bari, F. Zinna, *Chirality.* **2023**, *35*, 192–210.

Manuscript received: September 10, 2023
Accepted manuscript online: November 11, 2023
Version of record online: December 4, 2023